

# We are IntechOpen, the world's leading publisher of Open Access books Built by scientists, for scientists

6,900

Open access books available

186,000

International authors and editors

200M

Downloads

Our authors are among the

154

Countries delivered to

TOP 1%

most cited scientists

12.2%

Contributors from top 500 universities



WEB OF SCIENCE™

Selection of our books indexed in the Book Citation Index  
in Web of Science™ Core Collection (BKCI)

Interested in publishing with us?  
Contact [book.department@intechopen.com](mailto:book.department@intechopen.com)

Numbers displayed above are based on latest data collected.  
For more information visit [www.intechopen.com](http://www.intechopen.com)



## Near-Infrared Single-Photon Detection

Guang Wu, E Wu, Xiuliang Chen,  
Haifeng Pan and Heping Zeng  
*State Key Laboratory of Precision Spectroscopy,  
East China Normal University  
China*

### 1. Introduction

With the rapid increase of research interest in quantum information (Bennett&Brassard, 1984; Gisin et al., 2002; Knill et al., 2001), the near-infrared single-photon detection received a great boost not only in inventing (or improving) basic devices, but also in improving operation techniques on the conventional devices. Especially, in the application of quantum key distribution (Bennett&Brassard, 1984; Gisin et al., 2002), practical single-photon detectors (SPDs) with small size, operating at room-temperature are in great need.

Avalanche photodiodes (APDs) are usually used to build SPDs. Avalanche photodiodes (APDs) have internal gain due to a process of impact ionization that leads to multiple electron-hole pairs per input photon. Applying a large reverse voltage to the APD will result in a large multiplication gain, until the breakdown voltage ( $V_{br}$ ) is reached. Usually, the output photocurrent of the APDs is linearly proportional to the intensity of the optical input when the bias voltage is below  $V_{br}$ , and this mode is called as "linear mode". When the bias voltage is larger than  $V_{br}$ , the electron-hole generation process can become self-sustaining and result in a runaway avalanche, then a single photoexcited carrier can induce a runaway avalanche that gives rise to a detectable macroscopic current, and this mode is called as "Geiger mode". Si-APD SPD exhibits excellent performance with the spectral range from 400 to 1000 nm. Si APD is typically operated in free-running mode. Its detection efficiency is as high as 70% around 700 nm with the dark count rate (DCR) of 10-100 counts per second (Stipčević et al., 2010). InGaAs/InP APD has a spectrum response range from 1200 to 1700 nm, covering the fiber optical communication window at 1310 and 1550 nm. However, InGaAs/InP-APD SPD has a large dark count (e.g. DCR~ $10^5$  per second) and afterpulsing effect. Especially, the serious afterpulsing effect of the InGaAs/InP APD limits the application of high-speed detection. In order to improve its performance, an InGaAs/InP APD is usually operated in gated Geiger mode to suppress dark counts and afterpulsing effect. Recently, (Yuan et al., 2007; Namekata et al., 2006) reported self-cancellation and sine-wave techniques, which exhibited great improvements on the InGaAs/InP-APD SPD. The single-photon detection speed was increased significantly from megahertz to gigahertz.

Previously, it was thought that APDs are unable to resolve the number of photons in a short time interval. (Kardynal et al., 2008) first found that by suppressing the capacitive response down to a sufficiently low level, the weak avalanche current of an InGaAs/InP APD can be discriminated in its early development before saturated. In this mode, the variation in

multiplication gain of the current shows the capability of resolving photon number, called as “non-saturated” Geiger mode (Wu et al., 2009; Yuan et al., 2010). To date, some individual photon detectors have been demonstrated to exhibit interesting photon-number-resolving capability, such as visible light photon counters (Takeuchi et al., 1999), superconducting optical detectors (Miller et al., 2003; Schuster et al., 2007), and field effect transistors with quantum dots (Shields et al., 2000). All those developments have already stimulated vast promising applications although their performances are still limited by the requisite cryogenic operation.

On the other hand, several optical techniques have been developed to obtain high-performance near-infrared single-photon detection. A straightforward way to overcome the incapability of the current infrared detectors is to up-convert the infrared single photons with complete quantum state transfer into their replicas in the visual-near infrared region so that a Si-APD SPD can be used for the single-photon detection. Frequency up-conversion of 1550 nm single photons has been demonstrated by sum frequency mixing (Albota&Won, 2004; Pan et al., 2006). In particular, frequency up-converted single-photon detection facilitates a successful realization of a fiber-based QKD at gigahertz (Thew et al., 2006). Another optical technique for single-photon detection is just beginning (Han et al., 2008; Wu et al., 2010), where a high-gain optical amplifier is invented to amplify single photon to an intense light pulse. The spontaneous fluorescence is the major obstacle of the optical amplification technique to detect the single photon. (Han et al., 2008) used an optical parametric amplification, where the pulse width of the pump laser pulse was only 130 femtosecond. The influence of the spontaneous fluorescence was deeply suppressed in this ultra short period. (Wu et al., 2010) used a short optical bandpass filter to suppress the spontaneous fluorescence that few-photon pulse at 1550 nm could be detected.

In this chapter, we introduce some practical techniques of near-infrared single-photon detection, containing four sections as following: i) InGaAs/InP APD SPD; ii) Photon-number-resolving detector based on a InGaAs/InP APD; iii) Near-infrared single-photon detection with frequency up-conversion; iv) Few-photon detection with linear external optical gain photodetector.

## 2. InGaAs/InP-APD single-photon detector

The performance of an InGaAs/InP APD SPD is characterized by detection efficiency, dark count, afterpulsing effect, and time jitter, etc. The detection efficiency is mainly determined by two factors (Itzler et al., 2007): i) the quantum efficiency of the APD, which is the probability that a photon excited a carrier to reach the multiplication region, and ii) the avalanche breakdown probability, which figures the probability that a carrier in the multiplication region triggers an avalanche process successfully. The dark counts arise when carriers are created by processes other than photoexcitation, including the thermal excitation and field-mediated creation of free carriers (i.e. tunneling, trapping processes). Typically, the dark count rate of a Si-APD SPD is about 100 counts per second. However, the InGaAs/InP APDs have much more random bulk leakage carriers, leading to the dark count rate in the order of  $10^5$  counts per second. The afterpulsing effect is a dark count induced by the release of a carrier trapped by a defect in the multiplication region during an earlier avalanche event. In high-speed operation, the afterpulsing effect becomes the major problem that enhances dark counts. The time jitter is the variation in the temporal correspondence between the arrival of the photon and the detection of a resulting avalanche. It originates in

the stochastic nature of the carrier dynamics involved with avalanche breakdown, typically in the order of 100 ps for Si-APD APD.

In order to decrease dark counts and afterpulsing effect, InGaAs/InP APDs are usually operated in gated Geiger mode, by applying a reverse bias above the breakdown voltage with a short gating pulse over a DC bias. However, strong capacitive response of the electric gating pulse will be produced by the junction capacitance of the APD, which buries the weak avalanche pulses when a short gating pulse is used. It is quite important to produce an electric signal equal to the capacitive response of the APD, before cancelling the capacitive response. Here we present three different noise-cancellation techniques to operate the InGaAs/InP APD in gated Geiger mode with the gating width  $\leq 1$  ns.

### 2.1 Balanced capacitance cancellation technique

An equal capacitance can make a similar electric signal when it is applied on a same gate pulse, as most of the capacitive response is induced by the junction capacitance of the InGaAs/InP APD. Figure 1 is the frequency responses of a InGaAs/InP APD and a variable capacitance, where the InGaAs/InP APD is tested with a DC bias of 50 V. It seems similar between the InGaAs/InP APD and the variable capacitance below 500 MHz. So, capacitance is a simple and economical method to produce a similar capacitive response in a large frequency range. As shown in Fig. 2, a same electric pulse is both applied on the fiber pigtailed InGaAs/InP APD and the variable capacitance. The responses of the InGaAs/InP APD and the variable capacitance are sent to two differential inputs of a differential amplifier, respectively. The common signal such as the capacitive response is deeply suppressed in the differential amplifier, while the avalanche pulse is amplified. There were also several other cancellation techniques which suppressed the capacitive response effectively (e.g. (Bethune&Risk, 2000) produced a capacitive response by a coaxial cable reflection line; (Tomita& Nakamura, 2002) used two APDs to produce two capacitive responses).

The InGaAs/InP APD is cooled to  $-35$  °C. The width of the electric gating pulse is 1 ns with the gating rate of 25 MHz. A distribution feedback (DFB) laser diode is triggered at 1 MHz with the pulse duration  $< 300$  ps. The laser is synchronized at  $1/25$  of the electric gating pulse. And the laser pulses are attenuated to 0.1 photon per pulse before sent to the InGaAs/InP APD. The detection efficiency decreases with the bias voltage, seeing Fig. 3, and it becomes saturated at about 30%. However, the dark count and afterpulsing effect will degrade the detector when increase the bias voltage. As shown in Fig. 4, the dark count rate is less than  $8 \times 10^{-6}$  counts per gate at the detection efficiency of 10%. It exponential rises with the DC bias voltage until the detection efficiency of about 30%. Meanwhile, the afterpulsing effect is also measured with the detection efficiency. Figure 4 shows the afterpulsing probability at 40-ns delay after the first avalanche. It is less than 0.1% at the detection efficiency of 10%, and increases more slowly than the dark count rate below the detection efficiency of 25%. Then the afterpulsing effect dominates the dark count of the detector when the detection efficiency is close to 30%. The afterpulsing effect comes from the trapping effect in the multiplication region of the InGaAs/InP APD. The trapped carriers are exponential decay with time (Wu et al., 2006 ; Itzler et al., 2007). So the afterpulsing effect is the major obstacle for high speed operation, especially the adjacent two gating pulses should be less than 3 ns (Liang et al., 2011). Increasing the temperature of the InGaAs/InP APD can speed up the decay of the trapped carriers. However, it will obviously increase the dark count due to the thermal effect.

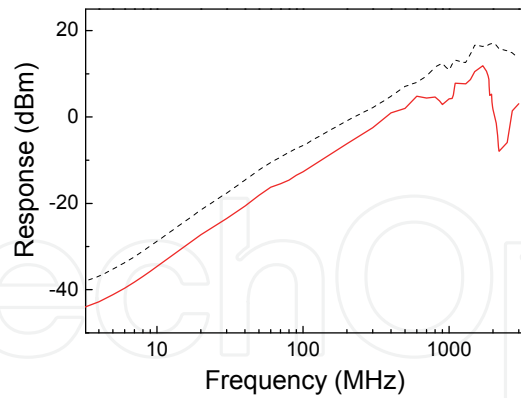


Fig. 1. Frequency response of an APD and a variable capacitance, where dash line: the APD, solid line: the variable capacitance

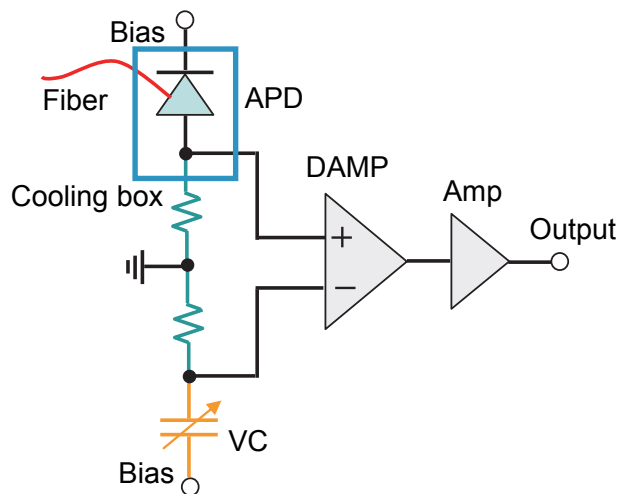


Fig. 2. Schematic of the balanced capacitance cancellation circuit, where Bias: DC bias + gating pulse, VC: a variable capacitance, DAMP: a differential amplifier, and AMP: a broadband amplifier

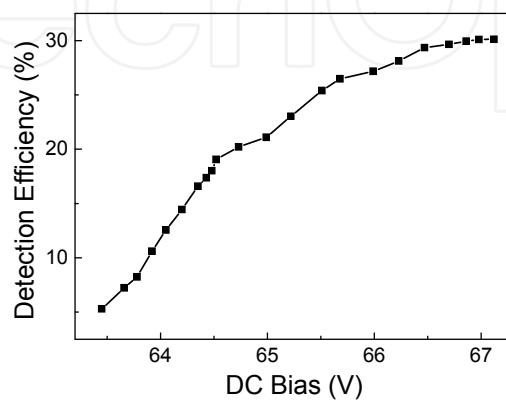


Fig. 3. Detection efficiency as a function of DC bias voltage

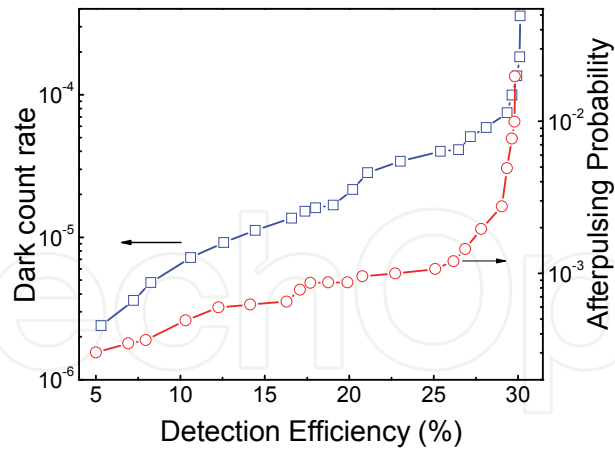


Fig. 4. Dark count rate and afterpulsing probability as a function of detection efficiency

Except rising the temperature, the other method to suppress the afterpulsing effect relies on decreasing the carriers passing through the APD, where shortening the gating width can decrease carriers. Figure 5 presents afterpulsing probability as a function of the gating width. It proves that short gating width is effective to suppress the afterpulsing effect for high speed operation.

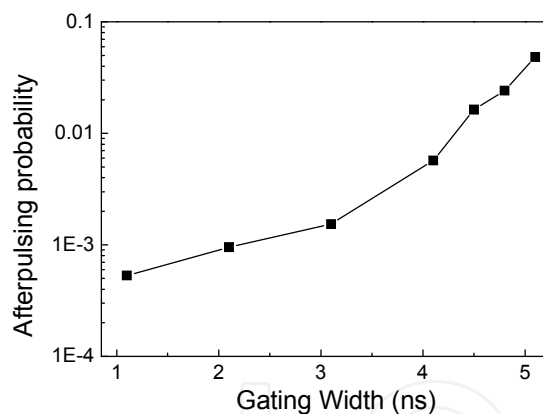


Fig. 5. Afterpulsing probability with the electric gating width

## 2.2 Self-cancellation technique

As mentioned above, shortening the gating width can decrease the number of bulk carriers passing through the InGaAs/InP APD, so it can weaken the afterpulsing effect for high speed operation. However, the avalanche current becomes weaker. It requires higher sensitivity, as well as better capacitive-response cancellation, to catch the avalanche pulse in the capacitive response. As shown in Fig. 1, the frequency responses between the InGaAs/InP APD and the variable capacitance are quite different when the frequency  $> 500$  MHz. So, the variable capacitance cannot produce absolutely same capacitive response with the InGaAs/InP APD, although it has a same value of the capacitance. The self-cancellation technique solves the problem nicely. Figure 6 is the schematic of this technique. The electric signal on the cathode of the InGaAs/InP APD is sent to a 50/50 power splitter to produce

two equal components. Then the two identical components are combined by a differencer, where one of the components is delayed by one gating period. The output of the differencer is the difference of the two components. Actually, they are the signals of two adjacent gating periods. The capacitive response is cancelled by itself. As a result, weak avalanche pulse can be discriminated at high-speed gating rate. (Yuan et al., 2010) promoted the gating rate as high as 2 GHz with the gating width of only 250 ps.

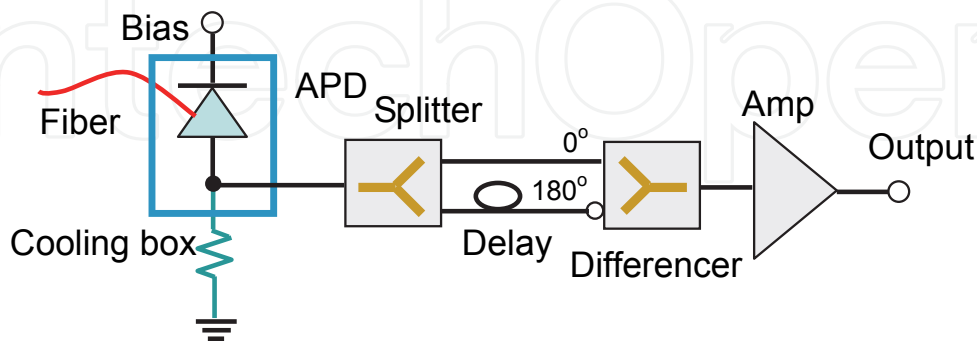


Fig. 6. Schematic of the self-cancellation circuit

### 2.3 Optical self-cancellation technique

In self-cancellation technique, the electric signal transmits through two coaxial cables. Due to the large transmission loss of the coaxial cable, the delay of one component cannot be too long; resulting in the gating rate should be high (e.g. > 200 MHz). Moreover, the electric circuit of the self-cancellation has a very wide bandwidth > 2 GHz. It should take more attention on designing and manufacturing for high cancellation ratio of the capacitive response. The optical self-cancellation technique gives a simple method to realize self-cancellation in wide bandwidth, including the operation at low gating rate.

Figure 7 is the schematic of the optical self-cancellation. The InGaAs/InP APD response is magnified by a low-noise broadband amplifier to trigger a DFB laser diode at 1550 nm. The response bandwidth of the laser diode is 2.5 GHz, fast enough to transfer the electronic signal to light pulse while keeping the same shape. In this way, the AC electronic signal is transformed to optical signal, preserving the original information from the InGaAs/InP APD including the capacitive response and the avalanche pulse. The fiber connecting the splitter and the detectors has different lengths to introduce a delay of one gating period between the two components. A fiber stretcher is employed to precisely control the delay

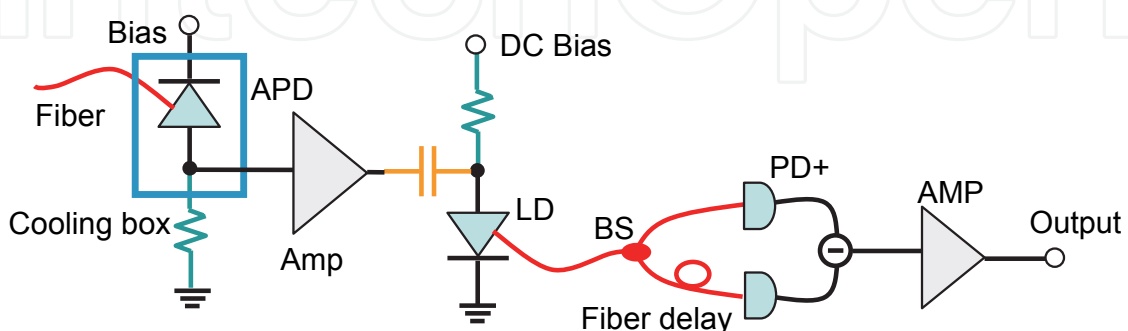


Fig. 7. Schematic of the optical self-cancellation circuit, where LD is a 1550-nm DFB laser diode, BS is a 50/50 fiber splitter, PD+ and PD- are the balanced optical detector

between the two components with 0.17-ps resolution. Two conventional photodiodes are used to detect the optical signals from each fiber. The response of the photodiodes exactly replayed the detection signal of the APD. At the output of the balancer, the identical capacitive response is subtracted. With this optical self-differential photodetector, the weak avalanche current can be measured (Wu et al., 2009).

### 3. Photon-number-resolving detection based on a InGaAs/InP APD

It was thought that a single APD cannot resolve the incident photon number without time or space multiplexing techniques since the gain on the APD is saturated in Geiger mode. However, recent research result reveals that the avalanche current is proportional to the photon number of the input light pulse when the APD is operated in non-saturated Geiger mode. Figure 8 gives a typical avalanche trace. It is recorded by a 6-GHz digital oscilloscope with the gating width of 5 ns. The current grows gradually first within area (a), and then it becomes saturated in area (b). Area (a) is the non-saturated Geiger mode period that the current is proportional to the input photon number. However, the saturation inhibits all the variation in the early avalanche development in area (b). The avalanche is just beginning in area (a), which the current is much weaker than the current in area (b). Through the optical self-cancellation technique, the non-saturated avalanche pulse is observed successfully.

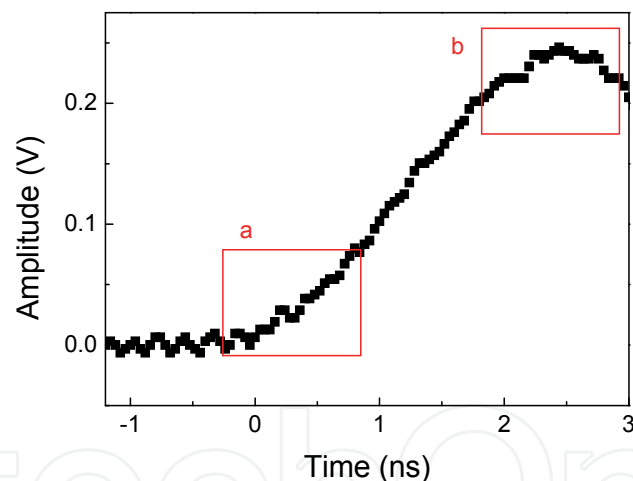


Fig. 8. An avalanche trace in 5-ns electric gate

Figure 9 is a typical histogram of the output peaks of the avalanche pulses. The distribution of the peak output of the avalanche pulses shows 3 peaks. Obviously, these distribution peaks are induced by different input photon number. The input light is from a DFB laser. This coherent light source obeys the Poissonian distribution, where the photon number ( $n$ ) is determined by the probability:

$$p(\mu, n) = \frac{\mu^n}{n!} e^{-\mu} \quad (1)$$

where  $\mu$  the is the mean photon number per pulse. The probabilities of the peak output of the avalanche pulses are calculated according to the Poissonian distribution, which is given by:

$$P(V) = \sum_{n=0}^{\infty} p(\mu, n) \cdot \rho(n, V) \quad (2)$$

where  $\rho(n, V)$  is the distribution of the peak output of the avalanche pulses when they are induced by  $n$ -photon. It shows a Gaussian-like distribution. The calculated data fits well with the measured data as shown in Fig. 9, proving that the avalanche current in non-saturated Geiger mode is proportional to the input photon number. The width of  $n$ -photon peak is  $\sqrt{n}$  ( $n > 1$ ) scaled to the 1-photon peak, which is caused by the statistical fluctuation. The width of 1-photon peaks is determined by the avalanche multiplication, and the excess noise derived from the statistical nature of the avalanche multiplication of the InGaAs/InP APD.

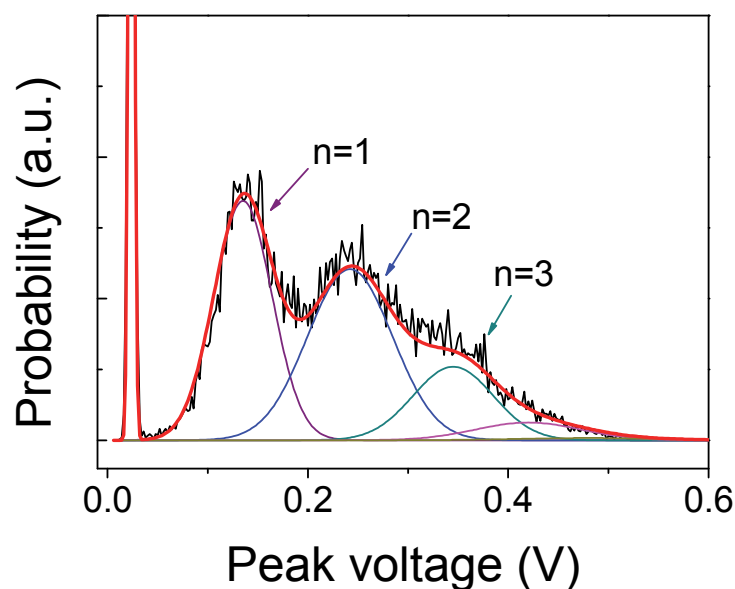


Fig. 9. Distribution of the peak output of the avalanche pulses, where the black line is the measured data, the red line is the calculated data. The detected mean photon number is 1.9 per pulse at the detection efficiency of 10%

Figure 10 is the color-grading waveforms of the avalanche pulses in non-saturated Geiger mode. It is recorded by a 6-GHz digital oscilloscope with the integration time of 0.1 second. Three peaks of the distribution of the avalanche pulses clearly appear in the waveforms. They are induced by 1-, 2-, and 3-photon, respectively.

Figure 8 shows that the non-saturated Geiger mode exits in a short period of the early avalanche development. As a result, in order to observe the capability of the photon-number-resolving (PNR) of the InGaAs/InP APD, the gating width should  $< 2$  ns. In order to figure out the relation between the PNR performance and the avalanche multiplication, the distributions of the peak output of the avalanche pulses at different detection efficiency are measured as shown in Fig. 11. It is hard to resolve the photon number at low detection efficiency. And the optimal period of the detection efficiency for PNR is from 10% to 20%.

When the detection efficiency increases to 36%, all the peak output of the avalanche pulses reach the maximum amplitude of 960 mV, the saturation effect appears obviously and the peak voltage is independent of the incident photon number more than 2. This sets the upper boundary for the InGaAs/InP APD to resolve photon numbers.

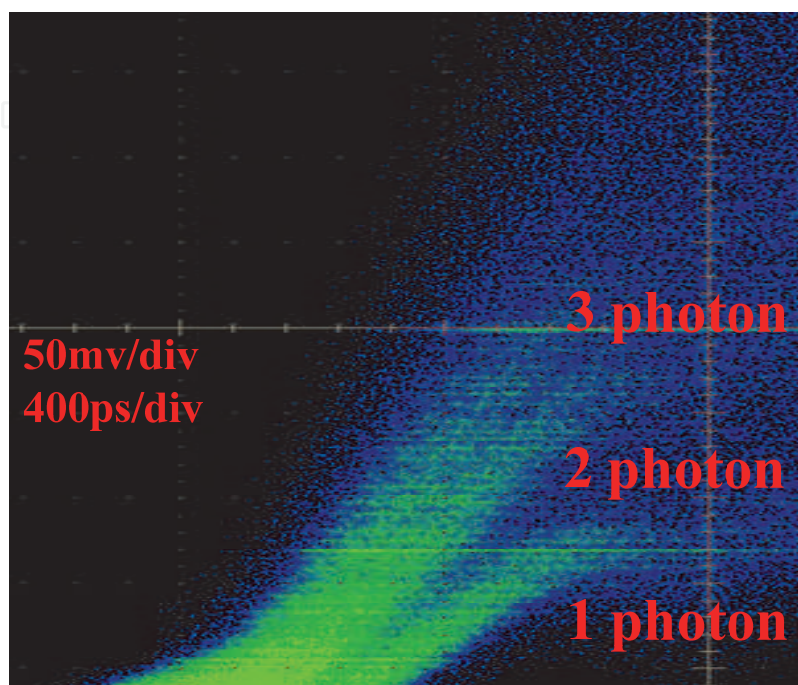


Fig. 10. Color-grading waveforms of the avalanche pulses

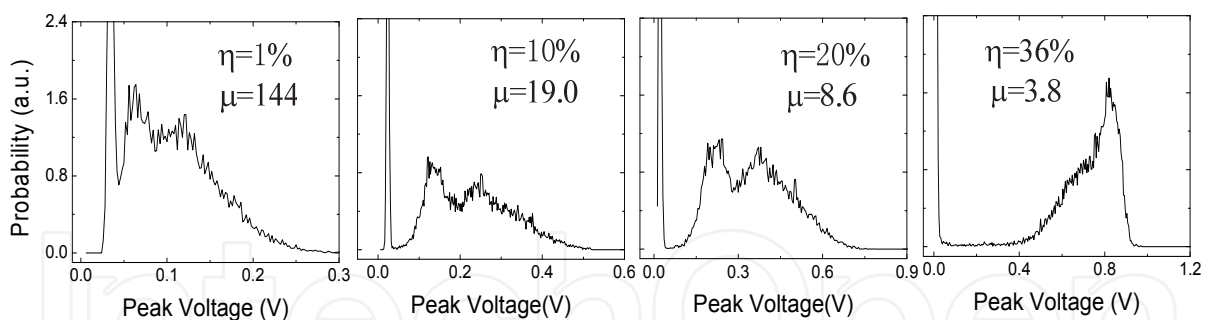


Fig. 11. Distribution of peak output of the avalanche pulses at different detection efficiencies

The PNR performance is time resolved with the input laser delay, since the non-saturated Geiger mode is observed in a short gated mode. Figure 12 shows the photon count rate varies with the laser pulse delay. The electric gating width is about 1.2 ns, while the effective detection gating width is about 300 ps. Three delays of the input laser are observed, they are signed as (a), (b), and (c) in Fig. 12. Figure 13 is the distribution of the peak output of the avalanche pulses at these three points. Obviously, the PNR performance is similar good at points (a) and (b). And the PNR performance degrades at point (c). As shown in Fig. 8, the avalanche multiplication gain increases for about 2 ns until saturated. So, the avalanche current obtains a larger gain when the photon arrives at the rising edge of the electric gate than that at the falling edge. Therefore, a large multiplication gain is good for PNR performance before the InGaAs/InP APD is saturated.

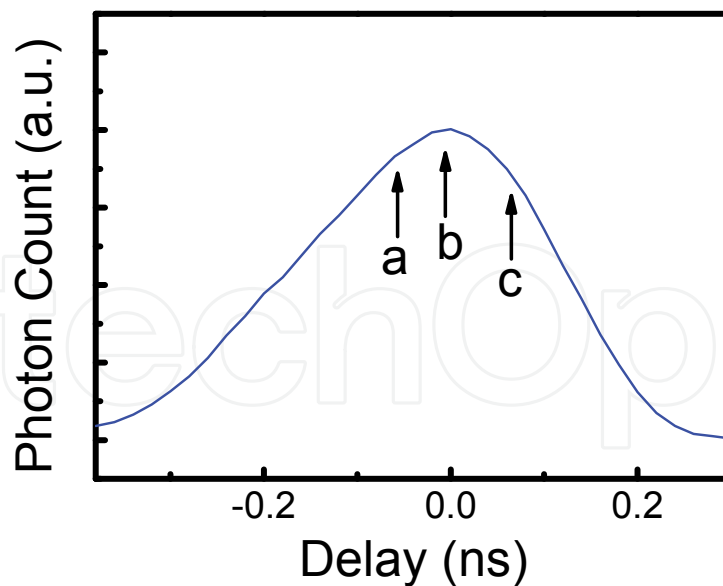


Fig. 12. Photon count rate as a function of the laser pulse delay

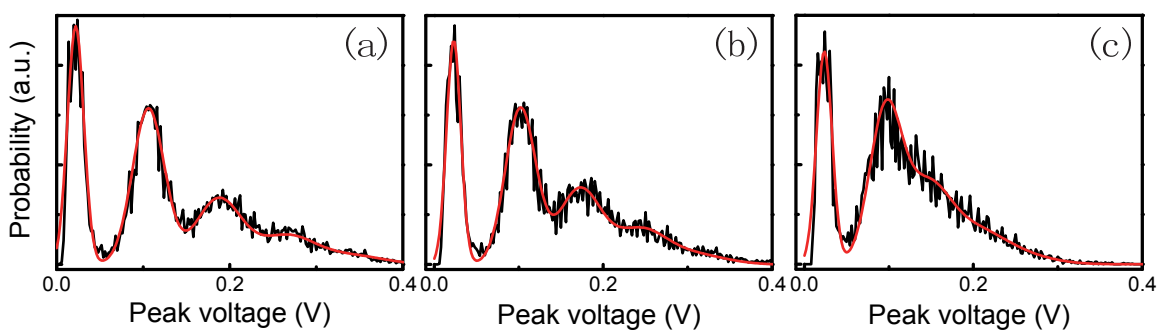


Fig. 13. Distribution of the peak output of the avalanche pulses at points (a), (b), and (c), respectively, where the detected mean photon numbers are 1.33, 1.35, and 1.32, respectively

#### 4. Near-infrared single-photon detection with frequency up-conversion

The single-photon frequency up-conversion can be considered as the sum-frequency generation (SFG) process as shown in Fig. 14. Suppose that the pump laser is in the single longitudinal mode. The solution to the coupled-mode equations for the phase-matched interaction is given by (Kumar, 1990):

$$\begin{aligned}\hat{a}_1(L) &= \hat{a}_1(0) \cos(|gE_p|L) - \hat{a}_2(0) \sin(|gE_p|L), \\ \hat{a}_2(L) &= \hat{a}_2(0) \cos(|gE_p|L) + \hat{a}_1(0) \sin(|gE_p|L),\end{aligned}\quad (3)$$

where  $\hat{a}_1$  and  $\hat{a}_2$  are annihilation operator for the signal and upconverted fields, respectively,  $g$  denotes the nonlinear coupling coefficient, and  $L$  is the length of the nonlinear medium. As indicated in Eq. (3), a complete quantum conversion occurs from  $\hat{a}_1$  to  $\hat{a}_2$  when  $|gE_p|L = \pi/2$  is satisfied. The single-photon conversion efficiency can be written as:

$$\eta = \sin^2(0.5\pi \cdot \sqrt{P_p / P_c}) \quad (4)$$

where  $P_p$  is the effective pump power, and  $P_c$  is the pump power at unity conversion efficiency.

The complete quantum conversion demands a large nonlinearity of the nonlinear media together with a strong pump field. Thus, periodically poled lithium niobate (PPLN) is usually employed in the single-photon frequency up-conversion since it has a large nonlinear coefficient ( $d_{eff} = 14 \text{ pm/V}$ ) and provides a large quasi-phase-matching (QPM) interaction length in the order of 10 mm. The single-photon frequency up-conversion has been demonstrated in a PPLN waveguide or bulk PPLN. With a PPLN waveguide, the requirement on the pump field power can be lowered since the power of the optical field can be confined to a small volume in the waveguide to have a very high intensity. The PPLN waveguide scheme requires subtle processes to prepare a monolithic fiber pigtailed PPLN waveguide, which will induce an avoidless big insertion loss (Tanzilli et al., 2002; Langrock et al., 2004&2005). And the bulk PPLN scheme requires a high pump power, e.g. using a resonant pump cavity with a stable cavity lock to enhance the circulating pump power (Albota et al., 2004); or enhancing single-photon frequency up-conversion by intracavity laser pump (Pan et al., 2006).

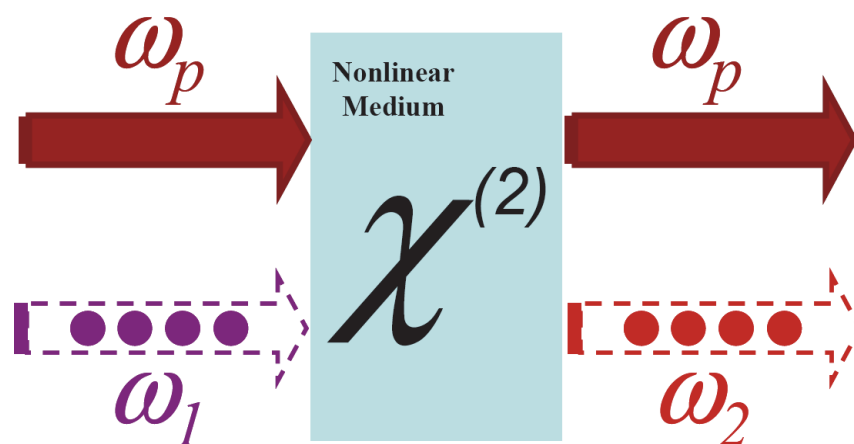


Fig. 14. Schematic of single-photon frequency up-conversion

For single-photon frequency up-conversion, one of the key parameters is the signal to noise ratio. If the noise is much larger than the signal photons, it will be meaningless to take the trouble to do the up-conversion. Therefore, suppressing the noise will much improve the performance of the single-photon frequency up-conversion in the applications. Figure 15 shows the possible noise sources in the intracavity enhanced up-conversion system discussed in the section above. The dark counts from the Si-APD SPD (10~200 counts per second depending on the device) could be neglected since the dark counts from the background photons are much larger. The main contribution to the background photons comes from the strong pump field. The background photons at 808 and 1064 nm comes from the solid-state laser itself. Besides the up-conversion process with the incident single photons, other nonlinear effects also takes place in the nonlinear media, such as second harmonic generation (SHG) of the pump laser at 532 nm and the optical parametric generation (OPG) fluorescence. These background photons could be removed by the filter system since they are at different wavelengths from the signal photons. However, among the background photons, there are some of the same wavelengths with the signal photons at 631 nm. They are caused by up-conversion of the parametric fluorescence caused by the

strong pump field. At first, spontaneous down-conversion of the strong pump took place in the nonlinear media as  $\omega_{1064\text{nm}} = \omega_{1550\text{nm}} + \omega_{3400\text{nm}}$ . In this process, the parametric fluorescence photons at 1550 nm are of the same wavelength with the incident signal photons. And since the temperature of the nonlinear media is tuned for the phase matching of SFG for  $\omega_{1064\text{nm}} + \omega_{1550\text{nm}} = \omega_{631\text{nm}}$ , these noise photons are up-converted together with the incident signal photons with high efficiency. Therefore, some of the output photons at 631 nm are not the replica of the incident signal photons but the noise from the up-converted parametric fluorescence. Unfortunately, these background photons can not be removed spectrally by the filters and contributed a lot to the dark counts on the Si-APD SPD.

Several groups have proposed the long-wavelength pump scheme to overcome the troublesome up-converted parametric fluorescence (Langrock et al., 2004; Dong et al., 2008; Kamada et al., 2008). By choosing a comparatively long-wavelength pump, which means the energy of the pump photons is lower than that of the signal photons, the parametric fluorescence from the down conversion will not fall in the incident infrared signal photon spectral regime. As a result, the pump induced parametric fluorescence can be efficiently suppressed and the dark counts will be greatly lowered. We have demonstrated an efficient single-photon frequency up-conversion system for the infrared photons at 1064 nm with ultralow dark counts (Dong et al., 2008). The pump source was provided by a mode-locked erbium-fiber laser. The repetition rate of the pulse train was 15.8 MHz and the pulse duration was measured to be 1.4 ps. The average output power of the amplifier was measured to be 27 mW. The peak power of the pulsed laser was  $\sim 220$  W, high enough to achieve unity conversion efficiency in the system. With such a pulsed pump source, no cavity enhancement was required, much simplifying the whole system. A long-pass filter with 1000 nm cutting off was placed in front of the PPLN crystal to block the stray light from the erbium doped fiber amplifier (EDFA), such as the pump for the EDFA from the LD at 980 nm and the green and red up-conversion emission of the EDFA. In this long-wavelength pump system, the relatively lower energy pump photon would not induce undesired parametric fluorescence at the signal wavelength 1550 nm, and the dark counts at SFG wavelength from followed up-conversion of the parametric fluorescence was eliminated. Moreover, besides that the Si-APD SPD did not respond to pump light at 1550 nm, the up-conversion fluorescence by the second harmonic of the strong pump was not phase matched at this working temperature, thus the noise from that process could also be ignored. Thanks to sufficient suppression of the intrinsic background photons, the narrow bandpass filter was even not necessary in the filtering system, increasing the transmittance of the filtering system. After the filtering system, we measured the dark counts of the whole detection system and got a count rate of  $\sim 150$  counts per second, when there were neither signal nor pump photons feeding. Moreover, when there was pump feeding, the dark count rate was still around 150 counts per second, indicating that the dark counts were not from the nonlinear parametric processes caused by the strong pump but mainly due to dark counts of Si-APD SPD and ambient background light. With this system, we achieved so far the lowest noise to efficiency ratio of  $\sim 160$  for a near unity conversion efficiency (93%) as shown in Fig. 16.

The single-photon frequency up-conversion has not only shown a solution to the sensitive detection of the infrared weak signals but also provided a technique to manipulate quantum states of the photons. Novel ideas on the techniques for single-photon frequency up-

conversion come forth from time to time, highlighting its applications in the quantum information processing.

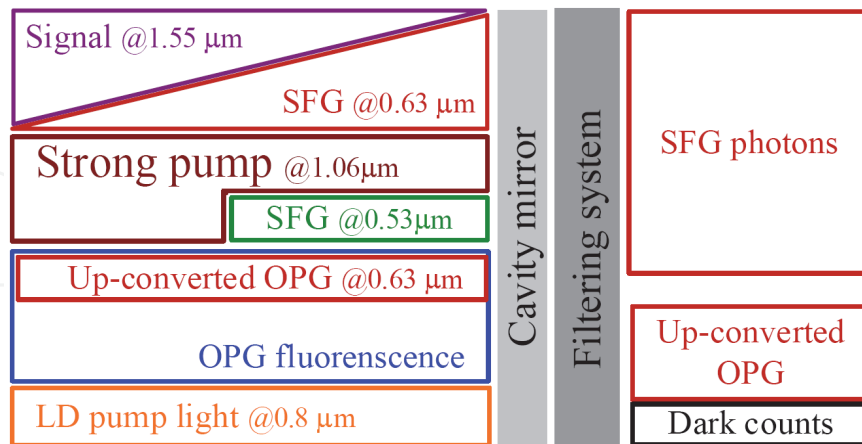


Fig. 15. Noise of the intracavity single-photon up-conversion

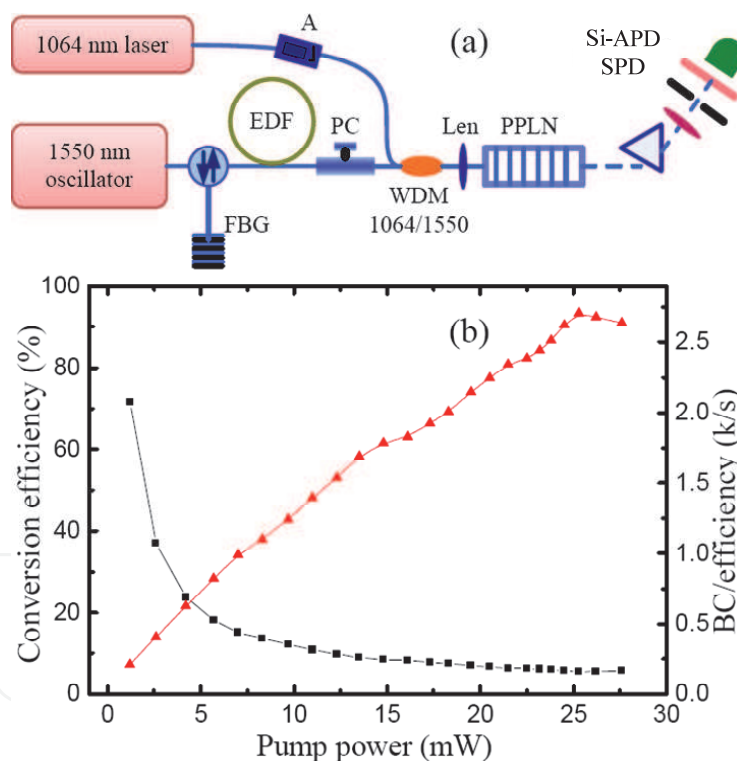


Fig. 16. Schematic of the long-wavelength pumped frequency up-conversion

## 5. Few-photon detection with linear external optical gain photodetector

Different from the most methods to amplify the photo-excited carrier with a large internal electric multiplication gain by electronic devices, we employed the optical devices to amplify the few-photon before detecting by a conventional PIN photodiode. Interestingly, the photodiode response showed a linear dependence on the incident photon signals, promising a novel few-photon detection technique.

Single-photon amplification by stimulated emission becomes the focus of research interest in recent years due to its application in quantum cloning (Simon et al., 2000; Fasel et al., 2002). In order to detect the amplified photon signals with conventional PIN photodiodes, the amplifier should be chosen under the constraint of a high gain. In addition, the amplifier noise due to the spontaneous emission should be suppressed enough to allow the identification of photons due to the stimulated emission. Er-doped optical fibers are commonly used in the optical fiber communication as amplifiers due to their large gain up to 40 dB around 1550 nm. But the spontaneous emission always accompanies the stimulated emission and will be amplified as well, which would be the big barrier to identify the signal photons from the noise. In order to suppress the amplified spontaneous emission (ASE), we separated the amplification into two steps. Figure 17(a) shows the setup of the external-gain photodetector based on the single-photon amplification. The light source is a laser diode modulated by an intensity modulator at 25.0 MHz with pulse duration of 325 ps. The output spectrum of the laser is shown by the green line in Fig. 18(b). The central wavelength is at 1550.20 nm and the full width at half maximum (FWHM) is 0.02 nm. The output of the laser is attenuated to contain only a few photons per pulse. Then, the photons are sent to the first EDFA for amplification. In order to detect the stimulated emission photons, spectral filtering is necessary because the ASE spectrum of the EDFA covered a broad range from 1527.36 to 1563.84 nm. Firstly, an inline bandpass filter (IF<sub>1</sub>) centered at 1550 nm with the FWHM of 3 nm is inserted to roughly extract the amplified signal photons from the broadband fluorescence.

Secondly, the combination of the two fiber Brag gratings (FBG<sub>1,2</sub>) with the FWHM of 0.18 nm form another bandpass filter. By tuning the temperature to combine the rising edge of FBG<sub>1</sub> and the falling edge of FBG<sub>2</sub>, a final bandwidth of the bandpass filter was determined to be 0.06 nm. Finally, a fiber polarization controller (PC) together with a polarization beam splitter (PBS) helps to remove the ASE noise of the orthogonal polarization. Then, the optical signal is sent to another EDFA for the amplification again. Since the incident photons are pre-amplified while most of the ASE noise is removed before the second amplification, the ASE of the second EDFA itself is much suppressed and instead the stimulated amplification is enhanced. Spectral filtering is not as strict as in the first step. The filtering system for the second amplification is composed of a bandpass inline filter (IF<sub>2</sub>) with the FWHM of 3 nm and a fiber Brag grating FBG<sub>3</sub> with the FWHM of 0.18 nm. The PBS is not even necessary in the second step because the ASE of the orthogonal polarization in the second EDFA is so weak that it could be ignored. The black line in Fig. 17(b) shows the ASE spectrum after the two-step amplification. The spectral width is mainly constrained by the combined FBG filters in the first step. When the signal photons are sent in, the peak at 1550.20 nm raises on the top of the ASE spectrum as shown by the red line in Fig. 17(b), indicating the stimulated amplification of the incident photons. The total gain of the two EDFAs is measured separately to be about 42.7 dB, indicating that an incident photon could be amplified to  $\sim 10^4$  photons per pulse (about 1 mW of the peak power) after the two-step amplification. The optical pulse signal is detected by a PIN photodiode. The variance of the ASE noise is measured and plotted as a function of the ASE output power as shown in Fig. 17(c). Since the main voltage noise is derived from the ASE beat on the PIN photodiode, the variance of the noise increased nonlinearly with the average output power, indicating that the ASE noise could be considered as a classical noise. The voltage noise amplitude is in Gaussian distribution with an FWHM of  $\sim 140$  mV (Fig. 17(d)).

Figure 18 plots the color-grading waveforms of the output voltage measured by the DPX acquisition mode of a 2.5-GHz oscilloscope with an average incident photon number of  $\mu = 4$

and 16. From the oscilloscope traces, it is observed that the peak output signal amplitude changes with the incident photon numbers, showing the evidence of the photon number resolving ability of the detector. The amplitude of the peak output signal shows a linear dependence on the input average photon number as shown in Fig. 20, indicating that the EDFAs and the photodiode are far from saturation under such milliwatt optical input power and capable of registering more than 16 individual photons. By taking into account the optical amplification, the photodiode response and the electronic amplification, the sensitivity of the whole setup is obtained by fitting the curve in Fig. 19 to be 15.39 mV/photon.

The photon statistics is studied by analyzing the histograms of the voltage signal acquired by the oscilloscope. The temporal resolution of oscilloscope is set to 100 ps, and the voltage amplitude resolution is set to 4 mV. A 500-ps sampling window is used in the analysis. Figure 20 plots the histograms of the peak output signal voltage recorded for different incident photon numbers of  $\mu = 4$  and 16 per pulse. The red lines in Fig. 21 show a simulation of the experimental data assuming a Poisson distribution for the incident photons. Due to the ASE noise variance, the distribution histograms are broadened, dimming the boundary for different photon numbers. By taking into account the Poisson distribution of the incident photons, the single photon response of the system is obtained to be 68 mV by fitting the curves in Fig. 20, and the quantum efficiency of the EDFAs is calculated to be 22.7%. Due to the linearity of the external-gain photodetector, the curves of the peak voltage kept the shapes of the ideal Poisson distribution of the input photons. The probability statistics of the peak output voltage could be also observed in Fig. 18 directly by its color-grading.

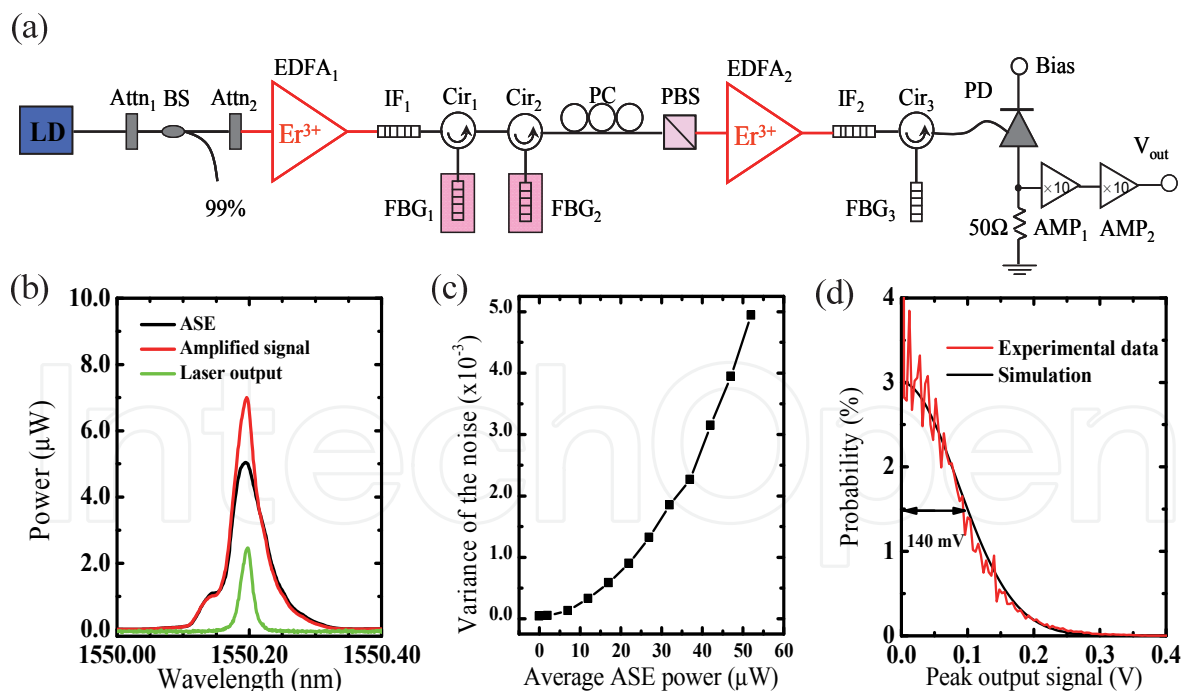


Fig. 17. (a) Schematic of the external-gain detector, where IF1,2: inline filters, FBG1-3: fiber Bragg gratings, Cir1-3: fiber circulators, PC: polarization controller, PBS: polarization beam splitter, PD: conventional pin photodiode, AMP: RF amplifiers. (b) Spectra of the laser (blue), ASE of the EDFA (green) and amplified single-photon signal (red). (c) variance of the ASE noise with the ASE power; (d) Distribution of the peak output of one photon.

Due to the larger spontaneous emission of the EDFA, the detector cannot discriminate single-photon pulses. The FWHM of the bandpass filter is 0.06 nm as well as about 7.4 GHz. The laser pulse width is  $\sim 325$  ps, corresponding to the laser bandwidth in the order of 10 GHz. The filter fits well with the laser pulse, but the insertion loss of the filters is about 15dB, most of them comes from FBG<sub>1</sub> and FBG<sub>2</sub>. So, more efforts are needed to suppress the spontaneous emission to decrease the insertion loss. However, the detector can be used as a sensitive power meter at single-photon level, as the integral output has a good linearity to the input photon number, while the noise is averaged.

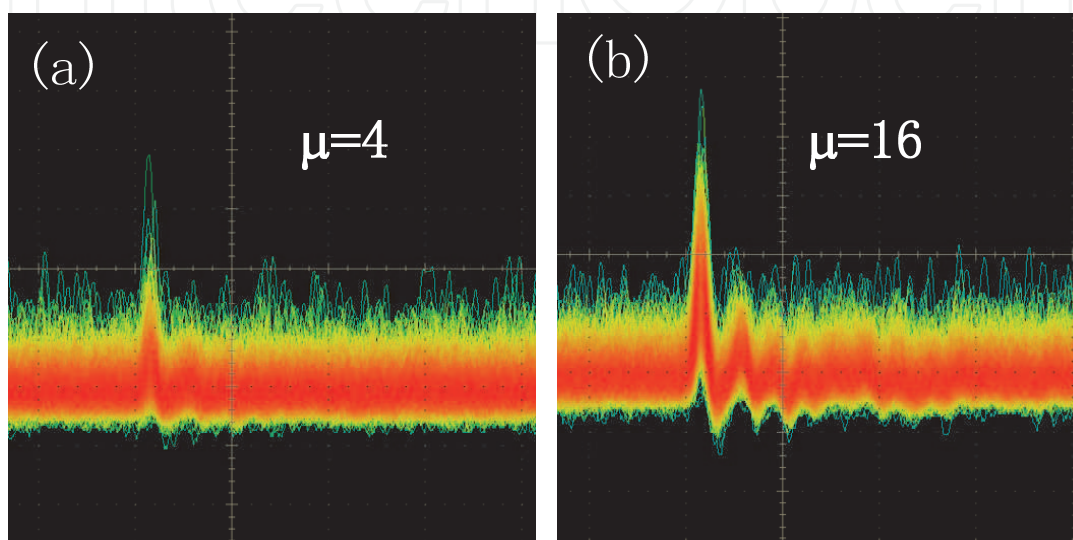


Fig. 18. Waveforms of the voltage output recorded by the oscilloscope with incident photon number of (a) 4 and (b) 16.

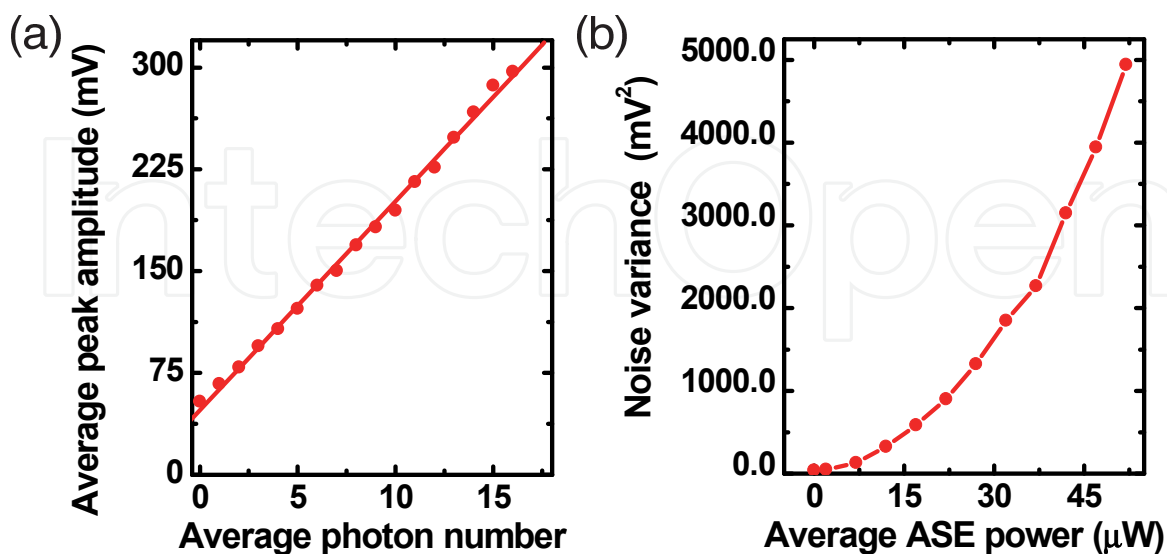


Fig. 19. Peak output voltage of the amplified photon signals and ASE noise variance. (a) Average peak amplitude as a function of the incident photon number. (b) ASE noise variance dependent on the output power.

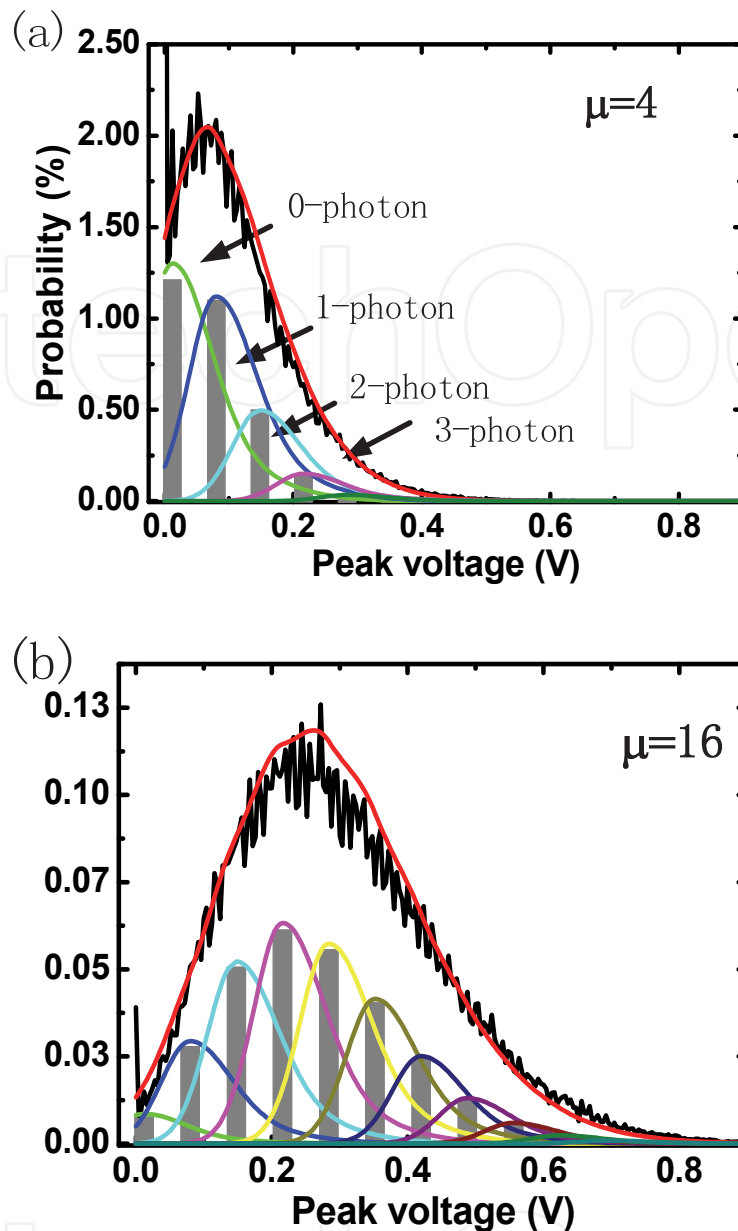


Fig. 20. Distributions of peak output signal for incident pulses of different average photon numbers, together with the calculated distributions

## 6. Conclusion

InGaAs/InP APDs are typically operated in gated Geiger mode for near-infrared single-photon detection. The afterpulsing effect becomes the major obstacle for high speed detection with the gating rate  $> 200$  MHz, which should use short gating width (e.g.  $\sim 1$  ns). The capacitive response of the InGaAs/InP APD must be cancelled to distil the weak avalanche pulse. We introduce three kinds of capacitive-response cancellation techniques, where the balanced capacitance cancellation technique is robust for operation at the gating rate  $< 200$ -MHz; and the self-cancellation and optical self-cancellation techniques are effective in higher gating rate up to 2 GHz. On the other hand, InGaAs/InP APDs are operated in non-saturated Geiger mode when the gating width  $< 2$  ns. In this mode, the

output of the InGaAs/InP APD is proportional to the input photon number. And we prove that the PNR performance is determined by the multiplication gain of the InGaAs/InP APD and input time of the photons.

Optical techniques are potential to realize high performance near-infrared single-photon detection. One of them is the single-photon frequency up-conversion. The major problem of up-conversion is the background photons induced by the optical nonlinear process, which could be resolved by using long-wavelength pump laser, and the background photons are suppressed at a negligible level. The other optical technique is just starting that detects few-photon pulse with a conventional linear photodiode after amplified by an external optical amplifier. Up to now, it still need efforts to realize an ultra-low noise optical amplifier for few-photon detection.

## 7. Acknowledgment

This work was funded, in part, by the National Natural Science Fund of China (10904039, 10525416, 10990101, and 91021014), Key Project Sponsored by the National Education Ministry of China (108058), Research Fund for the Doctoral Program of Higher Education of China (200802691032), and Shanghai Rising-Star Program (10QA1402100).

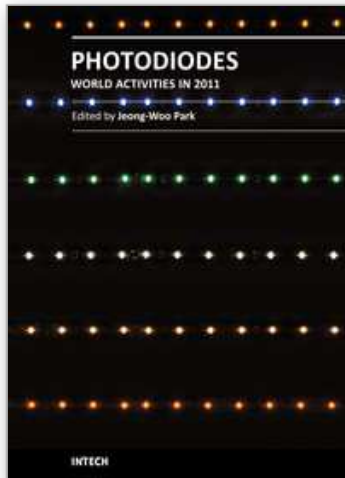
## 8. References

- Bennett, C. H. & Brassard, G. (1984). Quantum cryptography: Public key distribution and coin tossing. *Proc. IEEE Int. Conf. Comput. Syst. Signal Process.*, pp. 175-179
- Gisin, N.; Ribordy, G.; Tittel, W. & Zbinden, H. (2002). Quantum cryptography. *Rev. Mod. Phys.*, Vol.74, pp. 145-195
- Knill, E.; Laflamme, R. & Milburn, G. J. (2001). A scheme for efficient quantum computation with linear optics. *Nature* Vol.409, pp. 46-52
- Stipčević, M.; Skenderović, H. & Gracin, D. (2010). Characterization of a novel avalanche photodiode for single photon detection in VIS-NIR range. *Opt. Express*, Vol.18, pp. 17448-17459
- Yuan, Z. L.; Kardynal, B. E.; Sharpe, A. W. & A. J. Shields (2007). High speed single photon detection in the near infrared. *Appl. Phys. Lett.* Vol.91, 041114
- Namekata, N.; Sasamori, S. & Inoue, S. (2006). 800 MHz single-photon detection at 1550-nm using an InGaAs/InP avalanche photodiode operated with a sine wave gating. *Opt. Express*. Vol.14, pp. 10043-10049
- Kardynal, B. E.; Yuan, Z. L. & Shields, A. J. (2008). An avalanche-photodiode-based photon-number-resolving detector. *Nature Photonics* Vol.2, pp. 425-428
- Wu, G.; Jian, Y.; Wu, E; Zeng & H. P. (2009). Photon-number-resolving detection based on InGaAs/InP avalanche photodiode in the sub-saturated mode. *Opt. Express* Vol.17, 18782
- Yuan, Z. L.; Dynes, J. F.; Sharpe, A. W. & Shields, A. J. (2010). Evolution of locally excited avalanches in semiconductors. *Appl. Phys. Lett.* Vol.96, 191107
- Takeuchi, S.; Kim, J.; Yamamoto, Y. & Hogue, H. H. (1999). Development of a high-quantum-efficiency single-photon counting system. *Appl. Phys. Lett.* Vol.74, pp. 1063-1065

- Miller, A. J.; Nam, S. W.; Martinis, J. M. & Sergienko, A. V. (2003). Demonstration of a low-noise near-infrared photon counter with multiphoton discrimination. *Appl. Phys. Lett.* Vol.83, pp. 791-793
- Schuster, D. I.; Houck, A.; Schreier, J.; Wallraff, A.; Gambetta, J. M.; Blais, A.; Frunzio, L.; Majer, J.; Johnson, B.; Devoret, M. H.; Girvin, S. M. & Schoelkopf, R. J. (2007). Resolving photon number states in a superconducting circuit. *Nature* Vol.445, pp. 515-518
- Shields, A. J.; O'Sullivan, M. P.; Farrer, I.; Ritchie, D. A.; Hogg, R. A.; Leadbeater, M. L.; Norman, C. E. & Pepper, M. (2000). Detection of single photons using a field-effect transistor gated by a layer of quantum dots. *Appl. Phys. Lett.* Vol.76, pp. 3673-3675
- Albota, M. A. & Wong, F. N. C. (2004). Efficient single-photon counting at 1.55  $\mu\text{m}$  by means of frequency upconversion. *Opt. Lett.* Vol.29, 1449
- Pan, H. F.; Dong, H. F. & Zeng, H. P. (2006). Efficient single-photon counting at 1.55  $\mu\text{m}$  by intracavity frequency upconversion in a unidirectional ring laser. *Appl. Phys. Lett.* Vol.89, 191108
- Thew, R. T.; Tanzilli, S.; Krainer, L.; Zeller, S. C.; Rochas, A.; Rech, I.; Cova, S.; Zbinden, H. & Gisin, N. (2006). Low jitter up-conversion detectors for telecom wavelength GHz QKD. *New J. Phys.* Vol.8, 32
- Han, X. F.; Weng, Y. X.; Wang, R. Chen, X. H.; Luo, K. H.; Wu, L. A. & Zhao, J. M. (2008). Single-photon level ultrafast all-optical switching. *Appl. Phys. Lett.* Vol.92, 151109
- Wu, G.; Jian, Y.; Wu, E & Zeng, H. P. (2010). Linear external optical gain photodetector at few-photon level. *IEEE Photon. Tech. Lett.* Vol.22, pp. 688-690
- Wu, G.; Zhou, C. Y.; Chen, X. L. & Zeng, H. P. (2006). High performance of gated-mode single-photon detector at 1.55  $\mu\text{m}$ . *Opt. Comm.* Vol.265, pp. 126-131
- Itzler, M. A.; Ben-Michael, R.; Hsu, C. F.; Slomkowski, K.; Tosi, A.; Cova, S.; Zappa, F. & Ispasoiu, R. (2007). Single photon avalanche diodes (SPADs) for 1.5  $\mu\text{m}$  photon counting applications. *J. Mod. Opt.* Vol.54, pp. 283-304
- Bethune, D. S. & Risk, W. P. (2000). An autocompensating fiber-optic quantum cryptography system based on polarization splitting of light. *IEEE J. Quantum Electron.* Vol.36, pp. 340-347
- Tomita, A. & Nakamura, K. (2002). Balanced, gated-mode photon detector for quantum-bit discrimination at 1550 nm. *Opt. Lett.* Vol.27, pp. 1827-1829
- Liang, Y.; Jian, Y.; Chen, X. L.; Wu, G.; Wu, E & Zeng, H. P. (2011). Room-temperature single-photon detector based on InGaAs/InP avalanche photodiode with multichannel counting ability. *IEEE Photon. Tech. Lett.* Vol.23, pp. 115 - 117
- Yuan, Z. L.; Sharpe, A. W.; Dynes, J. F.; Dixon, A. R. & Shields, A. J. (2010). Multi-gigahertz operation of photon counting InGaAs avalanche photodiodes. *Appl. Phys. Lett.* Vol.96, 071101
- Kumar P. (1990). Quantum frequency conversion. *Opt. Lett.* Vol.15, pp. 1476-1478
- Tanzilli, S.; Tittel, W.; De Riedmatten, H.; Zbinden, H.; Baldi, P.; De Micheli, M.; Ostrowsky, D. B. & Gisin, N. (2002). PPLN waveguide for quantum communication. *Eur. Phys. J. D* Vol.18, pp. 155-160

- Langrock, C.; Diamanti, E.; Roussev, R. V.; Yamamoto, Y.; Fejer, M. M. & Takesue, H. (2004). Periodically poled lithium niobate waveguide sum-frequency generator for efficient single-photon detection at communication wavelengths. *Opt. Lett.* Vol.29, pp. 1518-1520
- Langrock, C.; Diamanti, E.; Roussev, R. V.; Yamamoto, Y.; Fejer, M. M. & Takesue, H. (2005). Highly efficient single-photon detection at communication wavelengths by use of upconversion in reverse-proton-exchanged periodically poled LiNbO<sub>3</sub> waveguides. *Opt. Lett.* Vol.30, pp. 1725-1727
- Dong, H. F.; Pan, H. F.; Li, Y.; Wu E & Zeng, H. P. (2008). Efficient single-photon frequency upconversion at 1.06  $\mu\text{m}$  with ultralow background counts. *Appl. Phys. Lett.* Vol.93, 071101
- Kamada, H.; Asobe, M.; Honjo, T.; Takesue, H.; Tokura, Y.; Nishida, Y.; Tadanaga, O. & Miyazawa H. (2008). Efficient and low-noise single-photon detection in 1550 nm communication band by frequency upconversion in periodically poled LiNbO<sub>3</sub> waveguides. *Opt. Lett.* Vol.33, pp. 639-641
- Simon, C.; Weihs, G. & Zeilinger, A. (2000). Optimal quantum cloning via stimulated emission. *Phys. Rev. Lett.* Vol.84, pp. 2993-2996
- Fasel, S.; Gisin, N.; Ribordy, G.; Scarani, V. & Zbinden, H. (2002). Quantum cloning with an optical fiber amplifier. *Phys. Rev. Lett.* Vol.89, 107901 (2002)

IntechOpen



## **Photodiodes - World Activities in 2011**

Edited by Prof. Jeong Woo Park

ISBN 978-953-307-530-3

Hard cover, 400 pages

**Publisher** InTech

**Published online** 29, July, 2011

**Published in print edition** July, 2011

Photodiodes or photodetectors are in one boat with our human race. Efforts of people in related fields are contained in this book. This book would be valuable to those who want to obtain knowledge and inspiration in the related area.

### **How to reference**

In order to correctly reference this scholarly work, feel free to copy and paste the following:

Guang Wu, E Wu, Xiuliang Chen, Haifeng Pan and Heping Zeng (2011). Near-Infrared Single-Photon Detection, Photodiodes - World Activities in 2011, Prof. Jeong Woo Park (Ed.), ISBN: 978-953-307-530-3, InTech, Available from: <http://www.intechopen.com/books/photodiodes-world-activities-in-2011/near-infrared-single-photon-detection>

**INTECH**  
open science | open minds

### **InTech Europe**

University Campus STeP Ri  
Slavka Krautzeka 83/A  
51000 Rijeka, Croatia  
Phone: +385 (51) 770 447  
Fax: +385 (51) 686 166  
[www.intechopen.com](http://www.intechopen.com)

### **InTech China**

Unit 405, Office Block, Hotel Equatorial Shanghai  
No.65, Yan An Road (West), Shanghai, 200040, China  
中国上海市延安西路65号上海国际贵都大饭店办公楼405单元  
Phone: +86-21-62489820  
Fax: +86-21-62489821

© 2011 The Author(s). Licensee IntechOpen. This chapter is distributed under the terms of the [Creative Commons Attribution-NonCommercial-ShareAlike-3.0 License](#), which permits use, distribution and reproduction for non-commercial purposes, provided the original is properly cited and derivative works building on this content are distributed under the same license.

IntechOpen

IntechOpen